Out-of-time-order correlations and Floquet dynamical quantum phase transition

Sara Zamani,[1,*] R. Jafari,[1,2,3,†] and A. Langari[4,‡]

[1]*Department of Physics, Institute for Advanced Studies in Basic Sciences (IASBS), Zanjan 45137-66731, Iran*
[2]*School of Physics, Institute for Research in Fundamental Sciences (IPM), P.O. Box 19395-5531, Tehran, Iran*
[3]*Department of Physics, University of Gothenburg, SE 412 96 Gothenburg, Sweden*
[4]*Department of Physics, Sharif University of Technology, P.O. Box 11155-9161, Tehran, Iran*

(Received 22 January 2022; accepted 23 February 2022; published 10 March 2022)

Out-of-time-order correlators (OTOCs) progressively play an important role in different fields of physics, particularly in the nonequilibrium quantum many-body systems. In this paper, we show that OTOCs can be used to probe the Floquet dynamical quantum phase transitions (FDQPTs). We investigate the OTOCs of two exactly solvable Floquet spin models, namely, Floquet XY chain and synchronized Floquet XY model. We show that the border of driving frequency range, over which the Floquet XY model shows FDQPT, is signaled by the global minimum of the infinite-temperature time averaged OTOC. Moreover, our results manifest that OTOCs decay algebraically in the long time, for which the decay exponent in the FDQPT region is different from that in the region where the system does not show FDQPTs. In addition, for the synchronized Floquet XY model, which reveals FDQPT at any driving frequency depending on the initial infinite or finite temperature, the imaginary part of the OTOCs becomes zero whenever the system shows FDQPT.

DOI: 10.1103/PhysRevB.105.094304

I. INTRODUCTION

Recently, out-of-time-order correlation (OTOC) has gained much attention in the physics community across many different fields, due to its feasibility in experiments [1–8] and also its richness in theoretical physics [9–25]. Recent progress in the experimental detection of quantum correlations and in quantum control techniques applied to systems as photons, molecules, and atoms, made it possible to directly observe an OTOC in nuclear magnetic resonance quantum simulators [6,8] and trapped ion quantum magnets [5].

The OTOC was first introduced by Larkin and Ovchinnikov in the context of superconductivity [25]. Lately, it has been revitalized, because it propounds an interesting and different insight into physical systems [23]. Some of the most important results involve the dynamics of quantum systems [9–14] such as quantum information scrambling [14–22,26] and quantum entanglement [15,24,27]. The decay of OTOC is closely related to the delocalization of information and implies the information-theoretic definition of scrambling. Scrambling is a process by which the information stored in local degrees of freedom spreads over the many-body degrees of freedom of a quantum system, becoming inaccessible to local probes and apparently lost. A connection between the OTOC and the growth of entanglement entropy, at the infinite temperature, in quantum many-body systems has also been discovered quite recently [15,24].

In addition, the study of OTOC has renewed the interest in the correspondence between classical and quantum chaos [28–34] with some analytical advances in the field of high-energy physics, mostly regarding the black hole information problem [35] and the Sachdev-Ye-Kitaev model [36]. OTOCs have been also developed into condensed-matter systems [37–41] as well as in statistical physics [42,43]. For instance, OTOC has been analyzed in conformal field theories [37], fermionic models with critical Fermi surface [44], weakly diffusive metals [37], Luttinger liquids [38], hard-core boson model [45], random field XX spin chain [46], symmetric Kitaev chain [47], and the $O(N)$ model [48]. In addition, it has been shown that OTOC equals the thermal average of the Loschmidt echo [49] and theoretically proposed that OTOC can be used as an order parameter to dynamically detect ergodic-nonergodic transitions [50,51], many-body localization transition [21,52], excited-state quantum phase transition [53,54], equilibrium quantum phase transitions [40,55,56], and quench dynamical quantum phase transitions (DQPTs) in many-body systems [1,40].

Despite considerable studies on OTOCs in a wide variety of quantum systems, comparatively little attention has been focused on the Floquet systems. In the present work, we study OTOCs in two Floquet spin systems, where both models show FDQPTs. In the first Floquet XY model, FDQPT occurs at any temperature within a finite range of driving frequency, where we show that the borders of the driving frequency window are captured by the global minimum of the infinite-temperature time averaged OTOCs. In other words, the time averaged OTOC can be used as an order parameter to detect the range of driving frequency over which FDQPTs occur. Moreover, the long-time behavior of OTOCs represents power-law decay

*sara.zamani@iasbs.ac.ir
†jafari@iasbs.ac.ir; raadmehr.jafari@gmail.com
‡langari@sharif.edu

with an exponent, which is different in the FDQPT and no-FDQPT regimes. Furthermore, in the synchronized Floquet XY model, the imaginary part of OTOCs, which is comprised of local and nonlocal operators, becomes zero when FDQPTs are present. It has to be mentioned that FDQPTs occur for any driving frequency at infinite or finite temperature in the latter model.

The paper is organized as follows: In the next section we define the OTOCs and some background materials. In Sec. III, we review the notion of dynamical quantum phase transition and its features. Section IV is dedicated to introducing the Floquet XY Hamiltonian, its FDQPT features, and discussing the OTOC behavior in the model. In Sec. V we first introduce the synchronized Floquet XY model and its FDQPT properties, and then we study the OTOC characteristics.

II. OTOCS

Consider a system with a Hamiltonian H, an initial state $|\psi\rangle$, and two local operators W_i and V_{i+r}, on sites i and $i+r$ of the system. The spreading of the operator W_i with time can be probed through the expectation value of the squared module of a commutator with a second operator V_{i+r},

$$C_{i,r}(t) = \tfrac{1}{2}\langle [W_i(t), V_{i+r}(0)]^\dagger [W_i(t), V_{i+r}(0)]\rangle, \tag{1}$$

where $W_i(t) \equiv e^{iHt} W_i(0) e^{-iHt}$ is the Heisenberg evolution of the operator W_i, and $\langle \mathcal{O}\rangle = \mathrm{Tr}(e^{-\beta H}\mathcal{O})/\mathrm{Tr}(e^{-\beta H})$ denotes averaging over the thermal ensemble with $\beta = 1/T$ the inverse temperature while setting the Boltzmann constant K_B to unity.

We consider a translational invariant system such that Eq. (1) depends only on the distance between two operators. Assuming operators W_i and V_{i+r} are both Hermitian and unitary, one can show that $C_r(t) \equiv C_{i,r}(t) = 1 - \mathrm{Re}[F_r(t)]$, in which $F_r(t) = \langle W_i(t) V_{i+r}(0) W_i(t) V_{i+r}(0)\rangle$ is dubbed OTOC for its unconventional time ordering [57,58]. From the operator delocalization assessment point of view, OTOC characterizes the spreading behavior of information. Vanishing $C_r(t)$ [or large $F_r(t)$] indicates that no information has traveled from site i to $i+r$ at time t.

In addition, $C_r(t)$ characterizes the quantum chaos via an exponential growth bounded by a thermal Lyapunov exponent. In classical physics, a hallmark of chaos is that a small difference in the initial condition results in an exponential deviation of the trajectory, i.e., $e^{\lambda_L t}$ where λ_L is the Lyapunov exponent (butterfly effect). The OTOC could be considered as the overlap of two states $W_i(t)V_{i+r}(0)|\psi\rangle$ and $V_{i+r}(0)W_i(t)|\psi\rangle$, where $V_{i+r}(0)$ acts in different ways to affect the growth of the time-evolved operator $W_i(t)$. In other words, $C_r(t)$ explicitly exhibits the difference in the outcome when the order of two operations $V_{i+r}(0)$ and $W_i(t)$ is exchanged [5,39,59]. The exponential deviation of normalized OTOC from unity, i.e., $F_r(t) \sim 1 - \#e^{\lambda_L t}$ diagnoses the chaos and the so-called "butterfly effect" in a quantum many-body system. Unlike classical systems where the Lyapunov exponent λ_L is unbounded, in quantum systems it is bounded by $2\pi/\beta$ (assuming $\hbar = 1$) [21]. Those systems which saturate the aforementioned bound are called fast scramblers, with examples including black holes [60,61], fermionic models with critical Fermi surface [44], weakly diffusive metals [37], and the $O(N)$ model [48]. However, some systems do not show such exponential growth (e.g., Luttinger liquids [38] and many-body localized systems [16,52,62]), and hence are characterized as less chaotic or as slow scramblers. These many-body quantum systems include rich information to connect thermalization and information scrambling, and may also be related to the study of hiding information behind the black hole horizon.

A. OTOC in the one-dimensional spin-1/2 exactly solvable models

In the one-dimensional spin-1/2 models, which are exactly solvable by means of Jordan-Wigner transformation [63–70], the operators W and V are replaced by single-site Pauli matrices σ^α ($\alpha = \{x, y, z\}$), and consequently the OTOC is given by

$$F_r^{\mu,\nu}(t) = \left\langle \sigma_r^\mu(t)\sigma_0^\nu \sigma_r^\mu(t)\sigma_0^\nu \right\rangle, \tag{2}$$

where $\mu, \nu = \{x, y, z\}$ and $\sigma^\alpha(t) = e^{iHt}\sigma^\alpha e^{-iHt}$. Since the model is exactly solvable by means of Jordan-Wigner transformation, it is convenient to express Pauli matrices by fermionic operators,

$$\begin{aligned}
\sigma_m^x &= \sigma_m^+ + \sigma_m^- \\
&= \Pi_{l<m}(1 - 2c_l^\dagger c_l)(c_m^\dagger + c_m) = \Pi_{l<m} A_l B_l A_m, \\
\sigma_m^y &= -i\,(\sigma_m^+ - \sigma_m^-) \\
&= -i\,\Pi_{l<m}(1 - 2c_l^\dagger c_l)(c_m^\dagger - c_m) = -i\,\Pi_{l<m} A_l B_l B_m, \\
\sigma_m^z &= 2c_m^\dagger c_m - 1 = -A_m B_m,
\end{aligned} \tag{3}$$

where $A_m = c_m^\dagger + c_m$, $B_m = c_m^\dagger - c_m$, and $c_m^\dagger$ (c_m) is the fermionic creation (annihilation) operator.

In terms of Jordan-Wigner fermions, some spin operators are local and some become nonlocal. Local operator, i.e., σ_m^z, consists of fermions only located at site m, while $\sigma_m^{x,y}$ are nonlocal according to their connections with all fermions located before site m. It has been shown that the relation of two-point correlations and OTOCs of local operators is different from nonlocal ones [57,58,71–73]. All OTOCs can be expressed in terms of the thermal average of A_m and B_m sequences. So, we need to calculate the expectation values of long sequences of A_m and B_m fermion operators, which can be turned into the sum of all possible products of two-point correlation functions, using the Wick's theorem. It should be noted that conservation of the fermion parity via operators is necessary for using free-fermion calculations and Wick's theorem [57,58,74]. The basic time-dependent correlation functions, which should be calculated, are $\langle A_p(t)A_q\rangle$, $\langle A_p(t)B_q\rangle$, $\langle B_p(t)A_q\rangle$, and $\langle B_p(t)B_q\rangle$. Using the Fourier transformations, the mentioned correlators are

expressed as

$$\begin{aligned}
\langle A_p(t)A_q\rangle &= \frac{1}{N}\sum_k e^{ik(p-q)}\langle U_k^\dagger(t)(c_k^\dagger + c_{-k})U_k(t)(c_{-k}^\dagger + c_k)\rangle,\\
\langle A_p(t)B_q\rangle &= \frac{1}{N}\sum_k e^{ik(p-q)}\langle U_k^\dagger(t)(c_k^\dagger + c_{-k})U_k(t)(c_{-k}^\dagger - c_k)\rangle,\\
\langle B_p(t)A_q\rangle &= \frac{1}{N}\sum_k e^{ik(p-q)}\langle U_k^\dagger(t)(c_k^\dagger - c_{-k})U_k(t)(c_{-k}^\dagger + c_k)\rangle,\\
\langle B_p(t)B_q\rangle &= \frac{1}{N}\sum_k e^{ik(p-q)}\langle U_k^\dagger(t)(c_k^\dagger - c_{-k})U_k(t)(c_{-k}^\dagger - c_k)\rangle,
\end{aligned} \tag{4}$$

where $N+1$ is the size of the system and p, q denote the position of operators in the spin chain.

B. OTOC of local operators

As mentioned, OTOCs characterize the delocalization of operators, and the study of local operators plays a key role in this context. By means of Jordan-Wigner transformation [Eq. (3)], OTOC of local operators, $F_r^{zz}(t)$, is given by

$$F_r^{zz}(t) = \langle A_r(t)B_r(t)A_0B_0A_r(t)B_r(t)A_0B_0\rangle, \tag{5}$$

for the exactly solvable spin-1/2 chain. In the thermodynamic limit, the above relation could be computed using the Wick's theorem. In this calculation, $\langle A_p(t)A_q\rangle$ and $\langle B_p(t)B_q\rangle$ terms do not vanish and we must consider the combination of all two-point correlation functions constructed with A and B operators. We can simplify the calculation of Eq. (5) using the Pfaffian method [75], which can be expressed in terms of skew-symmetric matrix Φ.

$$F_r^{zz}(t) = \pm Pf(\Phi_{zz}) = \pm\sqrt{\mathrm{Det}(\Phi_{zz})}, \tag{6}$$

where Φ_{zz} is constructed from two-point correlation functions [Eq. (4)], $(\Phi_{zz})_{ij} = \langle X_iX_j\rangle$, where X_i is the ith element inside thermal average expression $F_r^{zz}(t)$ [Eq. (5)].

C. OTOC of nonlocal operators

As mentioned before, the dynamical correlation functions of nonlocal operators are qualitatively distinct from local ones [57,72,73,76,77]. For two-point correlation functions at nonzero temperature, the time dependent decaying of nonlocal operators, which is exponential, is more similar to thermal behavior, in comparison with the behavior of local operators, which is power law. There are three different types of nonlocal OTOCs corresponding to various combinations of local and nonlocal operators. It should be mentioned that the operators σ_μ^x and σ_μ^y change the fermion parity. So their Heisenberg evolution cannot be obtained simply from the free-fermion Heisenberg-evolved operators $A_\mu(t)$ and $B_\mu(t)$, because the Heisenberg evolution of the fermion operators are simple only when the proposed Hamiltonian in free-fermion language is fixed over the full Fock space, including both parity sectors. However, we can use the "double trick" to deal with this case [57,74], by defining the following quantity:

$$\Gamma_r^{\mu,\nu}(t) = \left\langle\left[\sigma_{N/2}^\mu(t)\sigma_{N-r}^\mu(t)\sigma_0^\nu\sigma_{(N/2)-r}^\nu\right]^2\right\rangle. \tag{7}$$

Introducing the function $\Gamma_r^{\mu,\nu}(t)$ results in parity cancellation due to pairing of operators; and so one can simply use the Wick's theorem to expand the full function. For large size system and considering the mirror symmetry $F_r^{\mu,\nu}(t) = F_{-r}^{\mu,\nu}(t)$, we have [57,74]

$$\begin{aligned}
\Gamma_r^{\mu,\nu}(t) &= \left\langle\left(\sigma_{N/2}^\mu(t)\sigma_{(N/2)-r}^\nu\right)^2\right\rangle\left\langle\left(\sigma_{N-r}^\mu(t)\sigma_0^\nu\right)^2\right\rangle\\
&= F_r^{\mu,\nu}(t)F_{-r}^{\mu,\nu}(t) = \left[F_r^{\mu,\nu}(t)\right]^2.
\end{aligned} \tag{8}$$

Therefore, to obtain $F_r^{xx}(t)$, $F_r^{xy}(t)$, and $F_r^{xz}(t)$, we need to calculate $\Gamma_r^{xx}(t)$, $\Gamma_r^{xy}(t)$, and $\Gamma_r^{xz}(t)$, respectively (see Appendix A). Then, we perform a similar procedure as in Sec. II B using the Pfaffian method of the appropriate antisymmetric matrices and finally obtain the OTOC of the nonlocal operator as

$$F_r^{\mu,\nu}(t) = \pm\sqrt{Pf(\Phi_{\mu,\nu})} = \pm[Det(\Phi_{\mu,\nu})]^{1/4}. \tag{9}$$

In this paper, we will study both local and nonlocal OTOCs of two exactly solvable Floquet spin-1/2 models to investigate the behavior of OTOC and its ability to capture the FDQPT.

III. DYNAMICAL QUANTUM PHASE TRANSITION

Recently, a new research area of quantum phase transition has been investigated in nonequilibrium quantum systems, called dynamical quantum phase transitions (DQPTs) as a counterpart of equilibrium thermal phase transitions [78,79]. DQPT represents a phase transition between dynamically emerging quantum phases, that occurs during the nonequilibrium coherent quantum time evolution under quenching [79–83] or time-periodic modulation of a Hamiltonian [84–91]. In DQPT the real time acts as a control parameter analogous to temperature in conventional equilibrium phase transitions. The DQPT is characterized by the nonanalytical behavior of dynamical free energy [49,53,78,79,86,92–99], which is defined as

$$g(t) = -\lim_{N\to\infty}\tfrac{1}{N}\ln|\mathcal{G}L(t)|^2.$$

Here, N is the system size and $\mathcal{G}L(t)$ is the Loschmidt amplitude, which is given by $\mathcal{G}L(t) = \langle\psi(0)|\psi(t)\rangle$, where $|\psi(0)\rangle$ and $|\psi(t)\rangle$ are the initial state of the system and its corresponding time evolved state at a later time t, respectively.

However, in experiments [100,101], to search the far-from-equilibrium theoretical concepts, the initial state in which a system is prepared, is a mixed state. This motivates one to propose the generalized Loschmidt amplitude (GLA) for mixed thermal states, which perfectly replicates the nonanalyticities manifested in the pure state DQPTs [102,103]. The GLA for a thermal mixed state is defined as follows:

$$\mathcal{G}L(t) = \mathrm{Tr}(\rho(0)U(t)),$$

where $\rho(0)$ is the mixed state density matrix at time $t = 0$, and $U(t)$ is the time-evolution operator.

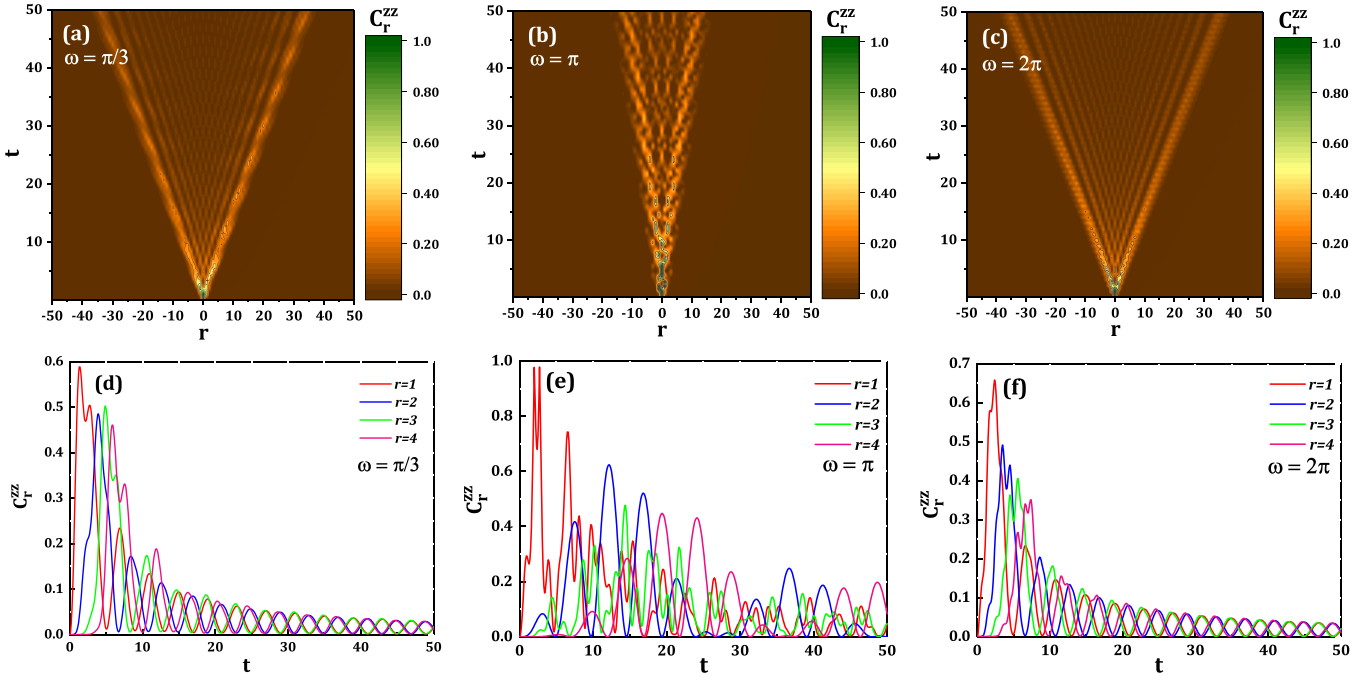

FIG. 1. Density plot of $C_r^{zz}(t)$ versus separation, r, and time, t, for (a) $\omega = \pi/3$, (b) $\omega = \pi$, and (c) $\omega = 2\pi$. The numerical simulation of the Floquet XY model is done for $N = 100$, inverse temperature $\beta = 0$, and $J = 0.25\pi$, $h = 0.5\pi$, and $\gamma = 0.5$, which shows FDQPT for $\pi/2 < \omega < 3\pi/2$. $C_r^{zz}(t)$ is plotted at fixed separations $r = 1, 2, 3, 4$ versus time and different driving frequency (d) $\omega = \pi/3$, (e) $\omega = \pi$, and (f) $\omega = 2\pi$.

IV. FLOQUET XY MODEL

The Hamiltonian of the one-dimensional periodically driving spin-1/2 chain, is given as follows:

$$\mathcal{H}(t) = \sum_{n=-N/2}^{N/2} \big\{[J-\gamma\cos(\omega t)]s_n^x s_{n+1}^x + [J+\gamma\cos(\omega t)]s_n^y s_{n+1}^y - \gamma\sin(\omega t)\big(s_n^x s_{n+1}^y + s_n^y s_{n+1}^x\big) + h s_n^z\big\}, \tag{10}$$

where $N+1$ is the size of the system, J, h, and γ are system parameters, and ω is the driving frequency. Here, S_n^α are the spin-1/2 operators at the nth site, i.e., $S_n^\alpha = \frac{1}{2}\sigma_n^\alpha$. In order to calculate the spin correlation functions, we should diagonalize the above Hamiltonian. The Hamiltonian can be exactly diagonalized by a Jordan-Wigner transformation, which transforms spins into spinless fermions. It should be mentioned that the fermionic representation of the Hamiltonian is equivalent to the one-dimensional p-wave superconductor with time-dependent pairing phase (magnetic flux) [85,86]. The Fourier transformed fermionic Hamiltonian can be expressed as the sum of independent terms $\mathcal{H}(t) = \sum_{k\in BZ} H_k(t)$, in which

$$H_k(t) = h_z(k)(c_k^\dagger c_k - c_{-k}c_{-k}^\dagger) - ih_{xy}(k)\big(e^{-i\omega t}c_k^\dagger c_{-k}^\dagger + e^{i\omega t}c_k c_{-k}\big), \tag{11}$$

where $h_z(k) = J\cos(k) + h$ and $h_{xy}(k) = \gamma\sin(k)$. The eigenstates and eigenvalues of the Hamiltonian, Eq. (11), are obtained by solving the time-dependent Schrödinger equation [84–86,89] (see Appendix B).

It is straightforward to show that the exact expression of the GLA is represented by [84,86]

$$\mathcal{G}L(t) = \Pi_k \mathcal{G}L_k(t),\ \ \mathcal{G}L_k(t) = \mathcal{R}(k,t) + i\mathcal{I}(k,t)\tanh(\beta\varepsilon_k),$$

with

$$\mathcal{R}(k,t) = \cos(\varepsilon_k t)\cos(\omega t/2) - \frac{B_z(k)}{\varepsilon_k}\sin(\varepsilon_k t)\sin(\omega t/2),$$

$$\mathcal{I}(k,t) = \sin(\varepsilon_k t)\cos(\omega t/2) + \frac{B_z(k)}{\varepsilon_k}\cos(\varepsilon_k t)\sin(\omega t/2),$$

where $B_z(k) = h_z - \omega/2$ and $\varepsilon_k = \sqrt{h_{xy}^2(k) + B_z^2(k)}$. It has been shown that the model shows FDQPTs, at any temperature, when the driving frequency ranges from $2(h-J)$ to $2(h+J)$, i.e., $2(h-J) < \omega < 2(h+J)$, where the system experiences adiabatic cyclic processes [84,85]. In the following we will examine the behavior of the OTOCs in the Floquet XY model to obtain their early and long-time scaling behavior.

A. OTOC of local operators in Floquet XY model

The OTOCs in the Floquet XY model can be obtained by lengthy and tedious calculation (see Appendix C). Figure 1 represents $C_r^{zz}(t)$ of the Floquet XY model versus time at infinite temperature, $\beta = 0$, for different values of driving frequency and $N = 100$. As seen, $C_r^{zz}(t)$ reveals a bounded cone structure (which indicates the bound of butterfly effect) with the velocity of wave front $c \approx 0.66$ for $\omega = \pi/3$ and 2π (no FDQPTs regime), and $c \approx 0.28$ for $\omega = \pi$ (FDQPTs regime). The numerical value of velocities is in good agreement with the maximum quasiparticle group velocities $(\partial\varepsilon_k/\partial k)$ of the

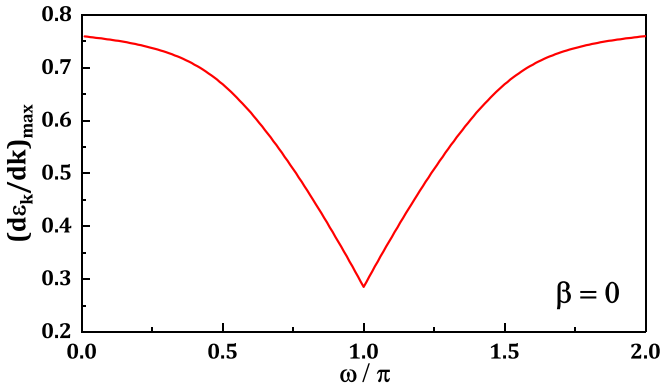

FIG. 2. The maximum quasiparticle group velocity of time-independent Floquet Hamiltonian Eq. (C1) versus ω/π. The maximum group velocity reaches a minimum at the middle of the driving frequency window, where the Floquet dynamical phase transition occurs.

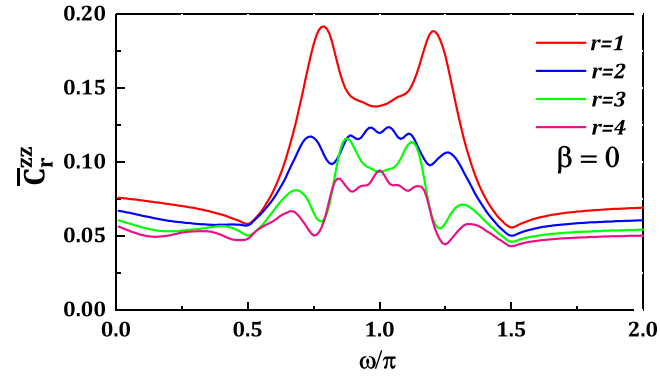

FIG. 4. Time average of C^{zz}_r versus driving frequency, for several fixed separations of the Floquet XY model and $N = 100$, in the presence of the periodically time-dependent Hamiltonian. The Hamiltonian parameters are $J = 0.25\pi$, $h = 0.5\pi$, and $\gamma = 0.5$.

effective time-independent Floquet Hamiltonian, Eq. (C1), at fixed frequencies [104]. The maximum quasiparticle group velocity of the effective time-independent Floquet Hamiltonian has been plotted in Fig. 2 versus ω. As seen, the maximum quasiparticle group velocity gets a minimum at the midfrequency of the region, where FDQPT occurs, namely, $\omega = \pi$. Comparing Figs. 1(a)–1(c) indicates that the system in the FDQPTs regime [Fig. 1(b)] reveals a narrower light cone with slower spreading of the local operator which expresses slower information propagating, witnessed by Fig. 2. This can be expected as the system evolves adiabatically in the FDQPTs regime [85], while the system experiences a nonadiabatic cyclic process in the no-FDQPTs regime. To accurately examine the behavior of $C^{zz}_r(t)$ for small value of separations r, $C^{zz}_r(t)$ has been depicted versus time in Figs. 1(d)–1(f). As seen, $C^{zz}_r(t)$ typically enhances in a short time from zero to its maximum value and then decreases to vanishing at long time in a periodic manner. Indeed, we observe that the OTOCs comprised of local operators show no sign of scrambling, namely, $\lim_{t\to\infty} C^{zz}_r(t) = 0$ (which is the same as the value at $t = 0$).

In addition, as is clear, the maximum value of $C^{zz}_r(t)$ decreases by increasing the separation r. So, it is important to probe how OTOC behaves at the early and the long times with fixed sites. The numerical simulation of $C^{zz}_r(t)$ is illustrated in Fig. 3 for separations $r = 1, 2, 3, 4$, and we can see clearly that the early time behavior is growing power law, t^{2r}, for any values of driving frequency. However, the long-time behavior represents t^{-1} decay in the no-FDQPTs regime ($\omega = \pi/3,\ 2\pi$), independent of r and β. In the FDQPTs regime ($\omega = \pi$) the long-time decaying behavior of $C^{zz}_r(t)$ is $t^{-2.6}$ and approximately disordered. Consequently, we expect that $C^{zz}_r(t)$ could show signatures to detect the range of driving frequency over which the FDQPT occurs. For this purpose we have calculated the infinite-temperature time average of $C^{zz}_r(t)$ as a function of frequency $\bar{C}^{zz}_r = \frac{1}{T}\int_0^T C^{zz}_r(t')dt'$, with $T = \frac{2\pi}{\omega}$. The numerical results have been illustrated in Fig. 4 for different r. As indicated, $\bar{C}^{zz}_r$ is roughly constant in the no-FDQPT regime while in the FDQPT regime it experiences large variation and its global minimums signal the boundary values of the window frequency over which the system shows FDQPTs. So, the time average of local OTOC can serve as a dynamical order parameter that dynamically detects the range of driving frequency over which FDQPTs occur. Moreover, the different long-time decaying behavior of $C^{zz}_r(t)$ at the FDQPT and no-FDQPT regimes can be interpreted as an indicator of nonadiabatic to adiabatic topological transition [85].

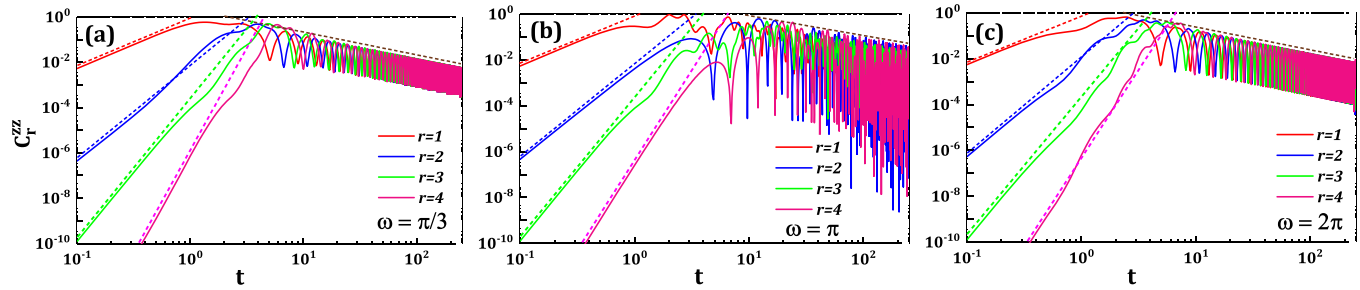

FIG. 3. The scaling behavior of C^{zz}_r versus time at fixed separation $r = 1, 2, 3, 4$ for the Floquet XY model, considering $N = 100$. The dashed lines are used for power-law fitting, which show t^{2r} power-law growth at early time, independent of the driving frequency, (a) $\omega = \pi/3$, (b) $\omega = \pi$, and (c) $\omega = 2\pi$. In addition, we see t^{-1} decaying behavior at long time, except for (b) which shows $t^{-2.6}$. The inverse temperature is $\beta = 0$ and the Hamiltonian parameters are $J = 0.25\pi$, $h = 0.5\pi$, and $\gamma = 0.5$.

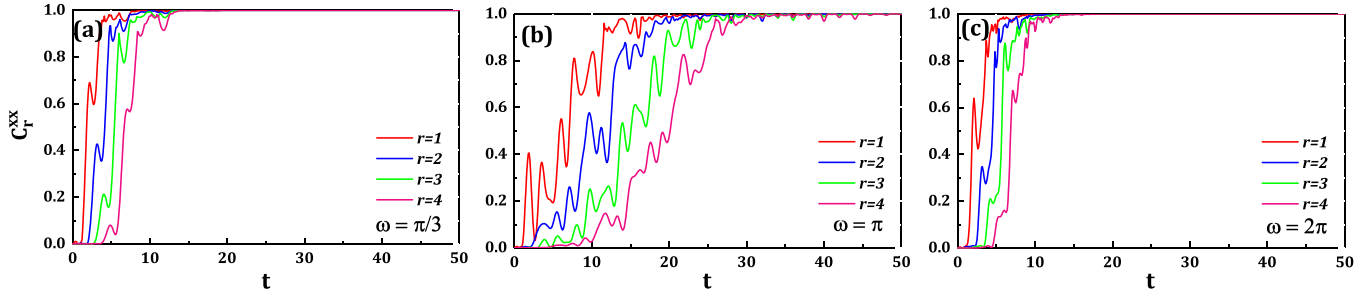

FIG. 5. Time evolution of nonlocal OTOC, C_r^{xx}, versus time for fixed separations $r = 1, 2, 3, 4$, of the Floquet XY model, with $\beta = 0$ and different values of driving frequency, (a) $\omega = \pi/3$, (b) $\omega = \pi$, and (c) $\omega = 2\pi$. The model parameters are $J = 0.25\pi$, $h = 0.5\pi$, $\gamma = 0.5$, and $N = 100$.

B. OTOC of nonlocal operators in Floquet XY model

As mentioned before, for an exactly solvable spin-1/2 model by means of Jordan-Wigner transformation, there are five kinds of OTOC of nonlocal operators. In Figs. 5(a)–5(c), $C_r^{xx}(t)$ has been depicted for $r = 1, 2, 3, 4$ in the FDQPT and no-FDQPT regimes. We can see that $C_r^{xx}(t)$ in both the FDQPT and the no-FDQPT regimes increases rapidly at short initial time from zero to reach its saturated value, 1. Since nonlocal operators bear nonlocal information about operators, the OTOCs comprised of nonlocal operators show the signature of scrambling which is their main difference compared with local ones. As can be seen from Fig. 5(b), enhancement of $C_r^{xx}(t)$ in the FDQPT regime is slower than that in the no-FDQPT regime, which means delocalization of information in the FDQPT regime occurs more slowly in comparison with the no-FDQPT case. Other OTOCs of nonlocal operators show similar behaviors (see Fig. 11 in Appendix C).

V. SYNCHRONIZED FLOQUET XY MODEL

The Hamiltonian of the synchronized Floquet XY model is given by [90]

$$H(t) = -\sum_{n=1}^{N}\left\{\frac{J(t)}{2}\left[(1+\gamma)\sigma_n^x\sigma_{n+1}^x + (1-\gamma)\sigma_n^y\sigma_{n+1}^y\right] + h(t)\sigma_n^z\right\}, \tag{12}$$

where $J(t) = \lambda h(t)$, $h(t) = h_0 + h_1\cos(\omega t)$, and γ represents the anisotropy. The Hamiltonian in Eq. (12) is exactly solvable by means of Jordan-Wigner transformation [90] (see Appendix D).

It has been shown that the GLA of the synchronized Floquet XY model is obtained to be [90]

$$\mathcal{G}L_k(t) = \cos(\epsilon_k\tau) + i\sin(\epsilon_k\tau)\tanh(|h(0)|\epsilon_k\beta), \tag{13}$$

where $\epsilon_k = \sqrt{P^2(k) + Q^2(k)}$, $P(k) = 2\lambda\cos(k) + 2$, $Q(k) = 2\lambda\gamma\sin(k)$, $\tau = \int_0^t h(t')dt'$, and $h(0) = h_0 + h_1$. The GLA becomes zero if the temperature goes to infinity, i.e., $\beta \longrightarrow 0$, at time instances $\tau^* = (2n+1)\pi/2\epsilon_k$ $(n = 0, 1, 2, \ldots)$. In addition, the FDQPTs occur for all temperatures if $h(0) = h_0 + h_1$ becomes zero, i,e., $h_0 = -h_1$. In other words, FDQPT in a synchronized Floquet system depends on the initial conditions, which occurs for all ranges of driving frequency and at any finite or infinite temperature. For simplicity and without loss of generality we consider the isotropic case $\gamma = 1$, which corresponds to the synchronized Floquet Ising model.

OTOC of local operators in the synchronized Floquet XY model

Firstly, we investigate the case in which our model shows FDQPTs at infinite temperature, i.e., the initial magnetic field is nonzero $h(0) \neq 0$. The local operator spreading in the synchronized Floquet XY model is probed by analyzing $F_r^{zz}(t)$, where its vanishing at long-time limit signals the information scrambling. Figure 6 shows numerical simulations of the real and imaginary parts of $F_r^{zz}(t)$ versus time and spin separation r for the synchronized Ising model $\gamma = 1$, at infinite $(\beta = 0)$ and finite $(\beta = 1)$ temperature with $N = 200$ and the strong synchronized coupling $\lambda = 1$. The real part of $F_r^{zz}(t)$, Fig. 6(a), reveals the bounded cone structure with the velocity of wave front $c = 2$. The situation for weak synchronized coupling $\lambda = 0.1$ is shown in Fig. 7, where the parameters of the model are the same as those in Fig. 6. As seen in Fig. 7, the diagrams of the real part of F_r^{zz} exhibit a narrower cone structure, representing slower spreading of local operators with the velocity $c = 0.2$. It indicates that the speed of operator spreading depends monotonically on the synchronized coupling strength.

It should be mentioned that, since the synchronized Floquet XY model cannot be transformed to the time-independent effective Floquet Hamiltonian (unlike the Floquet XY model), the quasiparticle group velocity cannot be defined here. So, the velocity of the wave front in the synchronized system cannot be related to the quasiparticle group velocity of the model. Moreover, it is clear that in both Figs. 6(b) and 7(b) the imaginary part of $F_r^{zz}(t)$ is zero at infinite temperature (the FDQPT case).

The numerical results have also shown that $\lim_{t\to\infty}\mathrm{Re}\{F_r^{zz}(t)\} = 1$, indicating no scrambling in OTOCs of local operator, analogous to that of the Floquet XY model. Although the qualitative behavior of $F_r^{zz}(t)$ at finite temperature (the no-FDQPTs case) is approximately similar to that at infinite temperature, the imaginary part of F_r^{zz} becomes nonzero at finite temperature independent of the synchronized coupling value [Figs. 6(c) and 7(c)].

Furthermore, analyzing the OTOCs of nonlocal operators has shown that the system is scrambled at infinite and finite temperature, which is expected from the nonlocal nature of inherited information (see Appendix E). At infinite temperature (the FDQPTs case), the

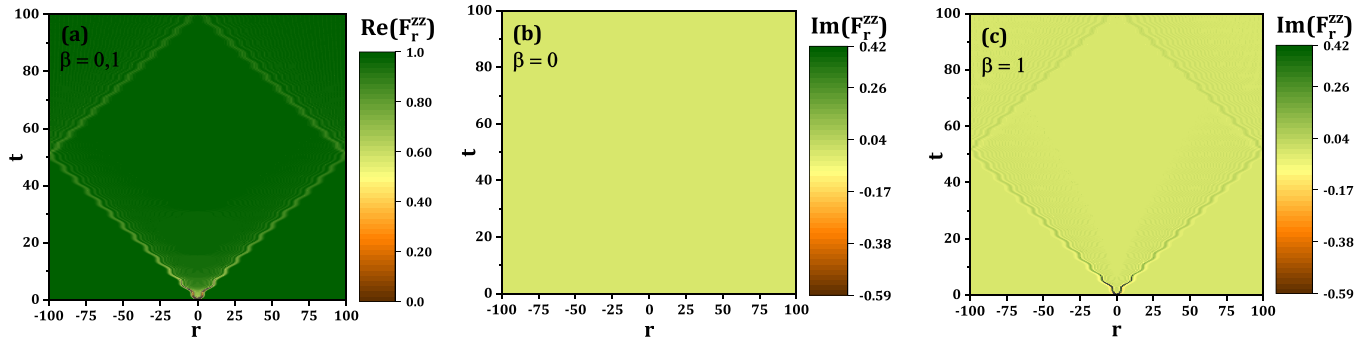

FIG. 6. Density plot of $F_r^{zz}(t)$ versus time and separation, for the synchronized Ising model at the strong coupling $\lambda = 1$, in the presence of $h(t) = h_0 + h_1 \cos(\omega t)$. (a) Real part of $F_r^{zz}(t)$ for both $\beta = 0, 1$. The imaginary part of $F_r^{zz}(t)$ for (b) infinite temperature $\beta = 0$ and (c) finite temperature $\beta = 1$. We consider $N = 200$ and Hamiltonian parameters are $h_0 = 1,\ h_1 = 1,$ and $\omega = \pi/2$.

imaginary part of OTOCs of nonlocal operators is also zero, while in the no-FDQPTs case (finite temperature) the imaginary part of OTOCs of nonlocal operators becomes nonzero.

As the second case, we consider $h(0) = 0$, where FDQPTs occur at any temperature for any values of driving frequency. The density plot of the real and imaginary parts of F_r^{zz}, are shown in Figs. 8 and 9 for strong and weak synchronized coupling $\lambda = 1$ and $\lambda = 0.1$, respectively. The numerical analysis exhibits that, the behavior of the real part of OTOCs of both local and nonlocal operators at infinite and finite temperature is the same. However, the imaginary part of OTOCs of both local and nonlocal operators vanishes at any temperature. Consequently, we come to the conclusion that the OTOCs with both local and nonlocal operators can be considered as a diagnostic tool to dynamically detect the FDQPTs in the synchronized Floquet XY model. In other words, the imaginary part of OTOCs becomes zero when the system undergoes the FDQPT.

Finally, to exactly assess how a local operator behaves dynamically and to verify its universal form, the evolution of C_r^{zz} for some fixed separations at finite and infinite temperature, has been depicted in Fig. 10. Since the interactions of Hamiltonian are local, we expect the power-law growth of C_r^{zz}, similar to previous studies [57,58]. As is clear, the short-time behavior of C_r^{zz}, in the case of $h(0) \neq 0$ [$h(0) = 0$] at any temperature, reveals the power-law trend t^n with position-dependent power $n \approx 4r - 3$ ($n \approx 10r - 3$), which has been extracted from the numerical results. Moreover, C_r^{zz} approaches its limiting value at long times, in a slow power law t^{-1}, independent of the value of separations and temperature.

VI. CONCLUSION

In this paper, we have studied the dynamical quantum phase transition of two periodically time driving Hamiltonians, the Floquet XY model and the synchronized Floquet XY model, via analyzing the behavior of out-of-time-order correlation. Our results indicate that out-of-time-order correlation is a proper diagnostic tool for studying the dynamical characteristics of quantum systems and can represent features of dynamical behavior. We discovered that out-of-time-order correlation of local operators could precisely detect the dynamical quantum phase transition. In the Floquet XY chain, the infinite-temperature time averaged out-of-time-order correlation of local operators can serve as a dynamical order parameter that dynamically detects the range of driving frequency over which FDQPTs occur. The aforementioned time average gets a jump with a minimum at the boundary of the FDQPT region. Moreover, the speed of the wave front of information spreading in the system becomes minimum in the region, which shows FDQPT. In the synchronized Floquet XY chain, it was indicated that vanishing of the imaginary part of OTOC signals the occurrence of dynamical quantum phase transition. In addition, the temperature dependence of the generalized Loshmidt echo comes from its imaginary part, which suggests that there is a connection between the real and imaginary parts of the generalized Loschmidt echo and those of the out-of-time-order correlation. Further investigations

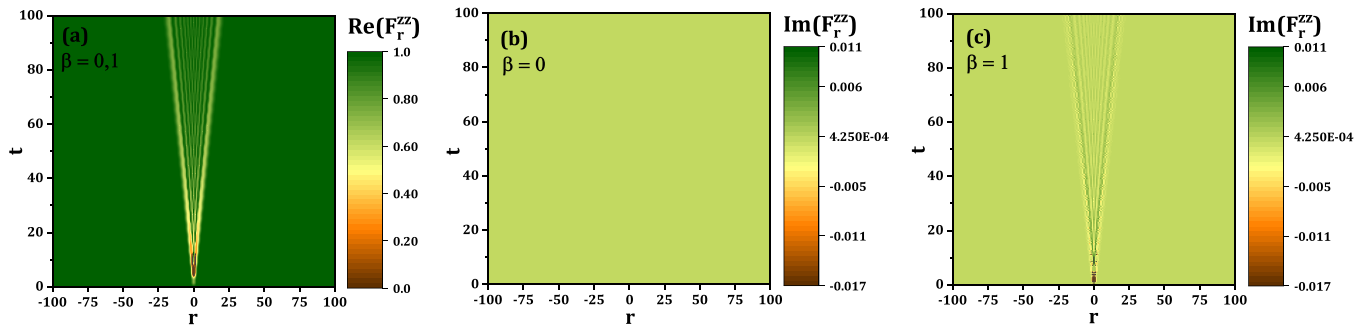

FIG. 7. Density plot of the real and imaginary parts of $F_r^{zz}(t)$ for weak coupling $\lambda = 0.1$ while other parameters are the same as in Fig. 6.

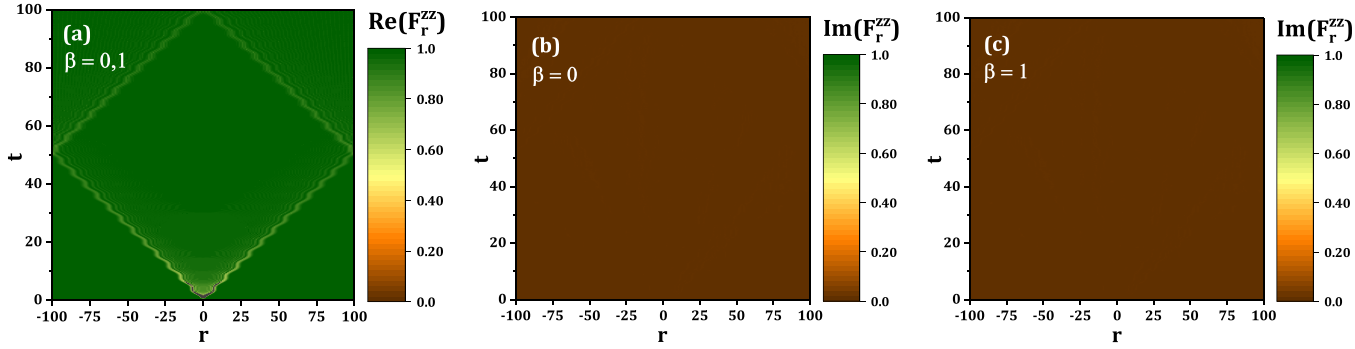

FIG. 8. Density plot of $F_r^{zz}(t)$ versus time and separation, for the synchronized Ising model at the strong coupling $\lambda = 1$, in the presence of $h(t) = h_0 + h_1 \cos(\omega t)$. (a) Real part of $F_r^{zz}(t)$ for both infinite and finite temperature $\beta = 0, 1$. (b) Imaginary part of $F_r^{zz}(t)$ for (b) $\beta = 0$ and (c) $\beta = 1$. The model is in strong coupling $\lambda = 1$ and $h_0 = 1$, $h_1 = -1$, $\omega = \pi/2$, and $N = 200$, which represents FDQPT at any temperature. The imaginary part of $F_r^{zz}(t)$ is always zero.

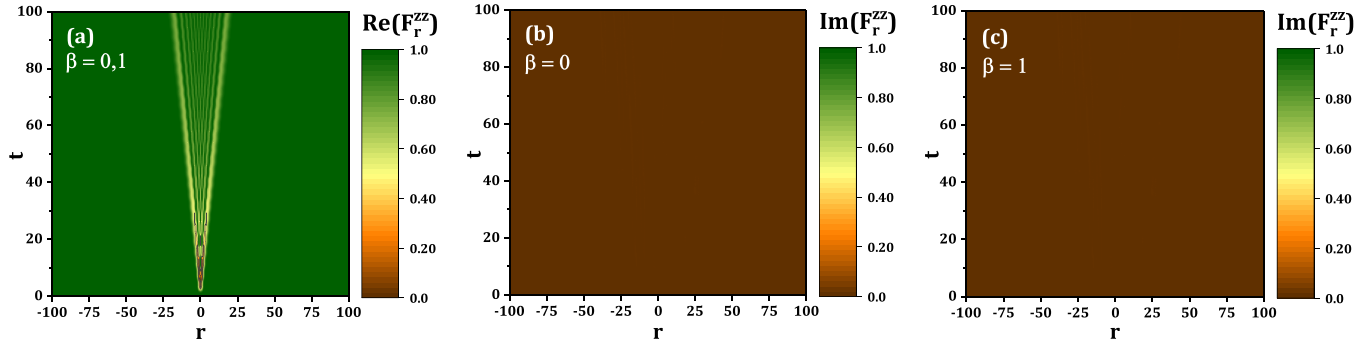

FIG. 9. Density plot of the real and imaginary parts of $F_r^{zz}(t)$ for weak coupling $\lambda = 0.1$ while other parameters are the same as in Fig. 8, with the imaginary part of $F_r^{zz}(t)$ zero everywhere in (b) and (c).

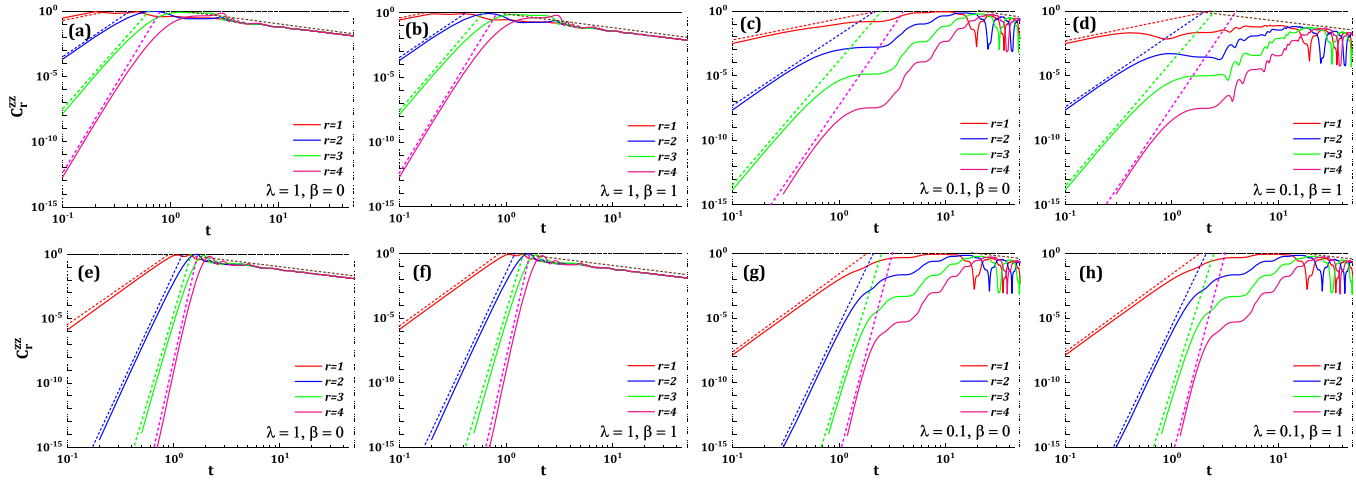

FIG. 10. Scaling behavior of C_r^{zz} with the universal form for several fixed separations of the synchronized Ising model, in the presence of $h(t) = h_0 + h_1 \cos(\omega t)$. The upper plots indicate the results of $h(0) \neq 0$ and the lower plots are for $h(0) = 0$. The dashed lines are used for power-law fitting. We see approximately t^{4r-3} (t^{10r-3}) power-law fashion at short times and t^{-1} decay at long times for the case of $h(0) \neq 0$ ($h(0) = 0$). We consider $N = 200$, frequency $\omega = \pi/2$, and Hamiltonian parameters $h_0 = 1$ and $h_1 = \pm 1$. The strong/weak coupling and infinite/finite temperature cases are (a) $\lambda = 1, \beta = 0$, (b) $\lambda = 1, \beta = 1$, (c) $\lambda = 0.1, \beta = 0$, (d) $\lambda = 0.1, \beta = 1$, (e) $\lambda = 1, \beta = 0$, (f) $\lambda = 1, \beta = 1$, (g) $\lambda = 0.1, \beta = 0$, and (h) $\lambda = 0.1, \beta = 1$.

would be interesting to establish a precise relation between the real and imaginary parts of the generalized Loschmidt echo and those of out-of-time-order correlation.

APPENDIX A: OTOC OF NONLOCAL OPERATORS

Using Eqs. (3) and (7), the expressions of $\Gamma_r^{xx}(t)$, $\Gamma_r^{xy}(t)$, and $\Gamma_r^{xz}(t)$ are written in the following forms:

$$\begin{aligned}
\Gamma_r^{xx}(t) &= \left\langle \left[\sigma^x_{N/2}(t)\sigma^x_{N-r}(t)\sigma^x_0\sigma^x_{(N/2)-r}\right]^2\right\rangle \\
&= \left\langle\left[\left(\prod_{l=N/2}^{N-r-1} B_l(t)A_{l+1}(t)\right)\left(\prod_{l=0}^{N/2-r-1} B_lA_{l+1}\right)\right]^2\right\rangle \\
\Gamma_r^{xz}(t) &= \left\langle \left(\sigma^x_{N/2}(t)\sigma^x_{N-r}(t)\sigma^z_0\sigma^z_{(N/2)-r}\right)^2\right\rangle \\
&= \left\langle\left[\left(\prod_{l=N/2}^{N-r-1} B_l(t)A_{l+1}(t)\right)\left(A_0A_{N/2-r}B_0B_{N/2-r}\right)\right]^2\right\rangle \\
\Gamma_r^{xy}(t) &= \left\langle \left(\sigma^x_{N/2}(t)\sigma^x_{N-r}(t)\sigma^y_0\sigma^y_{(N/2)-r}\right)^2\right\rangle \\
&= \left\langle\left[\left(\prod_{l=N/2}^{N-r-1} B_l(t)A_{l+1}(t)\right)\left(\prod_{l=0}^{N/2-r-1} A_lB_{l+1}\right)\right]^2\right\rangle.
\end{aligned} \tag{A1}$$

APPENDIX B: EXACT SOLUTION OF THE FLOQUET XY CHAIN

Considering the identity $\sum_{k\in BZ}\cos(k)=0$, one can rewrite Eq. (11) as follows:

$$\begin{aligned}
\mathcal{H}_k(t) &= h_z(k)(c_k^\dagger c_k + c_{-k}^\dagger c_{-k}) \\
&\quad - ih_{xy}(k)\left(e^{-i\omega t}c_k^\dagger c_{-k}^\dagger + e^{i\omega t}c_kc_{-k}\right) - h.
\end{aligned} \tag{B1}$$

It is convenient to use the following basis for the kth subspace, which is defined in the Heisenberg picture

$$|0\rangle,\quad c_k^\dagger|0\rangle,\quad c_{-k}^\dagger|0\rangle,\quad c_k^\dagger c_{-k}^\dagger|0\rangle. \tag{B2}$$

In this representation, the Hamiltonian $\mathcal{H}_k(t)$ can be expressed as

$$\mathcal{H}_k(t)=\begin{pmatrix} -h & ih_{xy}(k)e^{i\omega t} & 0 & 0 \\ -ih_{xy}(k)e^{-i\omega t} & 2h_z(k)-h & 0 & 0 \\ 0 & 0 & h_z(k)-h & 0 \\ 0 & 0 & 0 & h_z(k)-h \end{pmatrix}. \tag{B3}$$

By solving the time-dependent Schrödinger equation, we obtain the eigenvalues and eigenvectors of Hamiltonian $\mathcal{H}_k(t)$:

$$i\frac{d}{dt}|\psi_k^\pm(t)\rangle = \mathcal{H}_k(t)|\psi_k^\pm(t)\rangle. \tag{B4}$$

The exact solution of the Schrödinger equation is found by going to the rotating frame given by the periodic unitary transformation

$$U_R(t)=\begin{pmatrix} 1 & 0 & 0 & 0 \\ 0 & e^{-i\omega t} & 0 & 0 \\ 0 & 0 & 1 & 0 \\ 0 & 0 & 0 & 1 \end{pmatrix}. \tag{B5}$$

In the rotating frame the eigenstate is given by $|\chi_k^\pm(t)\rangle = U_R^\dagger(t)|\psi^\pm(k,t)\rangle$. Substituting the transformed eigenstate into the Schrödinger equation, the time-dependent Hamiltonian is transformed to its time-independent form $\mathcal{H}_k|\chi_k^\pm(t)\rangle = E^\pm|\chi_k^\pm(t)\rangle$ where

$$\mathcal{H}_k=\begin{pmatrix} -h & ih_{xy}(k) & 0 & 0 \\ -ih_{xy}(k) & 2h_z(k)-h-\omega & 0 & 0 \\ 0 & 0 & h_z(k)-h & 0 \\ 0 & 0 & 0 & h_z(k)-h \end{pmatrix}. \tag{B6}$$

The Hamiltonian $\mathcal{H}_k$ is in block-diagonal form, which leads to the following eigenvalues and eigenvectors:

$$\begin{aligned}
E_k^{1,2} &= \left(h_z(k)-h-\frac{\omega}{2}\right)\pm\varepsilon_k, \\
E_k^{3,4} &= h_z(k)-h,
\end{aligned} \tag{B7}$$

where $\varepsilon_k=\sqrt{[h_{xy}(k)]^2+[h_z(k)-\frac{\omega}{2}]^2}$ and

$$\begin{aligned}
|\chi_k^1\rangle &= \begin{pmatrix}\cos(\gamma_k/2)\\ \sin(\gamma_k/2)\end{pmatrix}, \\
|\chi_k^2\rangle &= \begin{pmatrix}\sin(\gamma_k/2)\\ -\cos(\gamma_k/2)\end{pmatrix},
\end{aligned} \tag{B8}$$

in which

$$\gamma_k = 2\arctan\left[\frac{h_z(k)-\frac{\omega}{2}-\varepsilon_k}{h_{xy}(k)}\right]. \tag{B9}$$

APPENDIX C: CALCULATION OF THE FLOQUET OTOC

To obtain the time evolution operator of Floquet Hamiltonian, $U_k(t)=U_R(t)U_F(t)$, we need to calculate $U_F(t)=e^{-i\mathcal{H}_kt}$. The upper-left block of $\mathcal{H}_k$ is given by $\mathcal{H}'_k$:

$$\begin{aligned}
\mathcal{H}'_k &= \begin{pmatrix} -h & ih_{xy}(k) \\ -ih_{xy}(k) & 2h_z(k)-h-\omega \end{pmatrix} \\
&= \left[h_z(k)-\frac{\omega}{2}-h\right]\mathbb{1}+\varepsilon_k\hat{h}_l(k)\cdot\vec{\sigma}.
\end{aligned} \tag{C1}$$

At first, we calculate $e^{-i\mathcal{H}'_kt}$,

$$\begin{aligned}
e^{-i\mathcal{H}'_kt} &= e^{-it[-h+h_z(k)-(\omega/2)]}e^{-it\varepsilon_k\hat{h}_l(k)\cdot\vec{\sigma}} \\
&= e^{-it[-h+h_z(k)-(\omega/2)]}[\cos(\varepsilon_kt)-i\sin(\varepsilon_kt)(\hat{h}_l(k)\cdot\vec{\sigma})] \\
&= e^{-it[-h+h_z(k)-(\omega/2)]}\begin{pmatrix}\cos(\varepsilon_kt)+i\frac{h_z(k)-\omega/2}{\varepsilon_k}\sin(\varepsilon_kt) & \frac{h_{xy}(k)}{\varepsilon_k}\sin(\varepsilon_kt) \\ -\frac{h_{xy}(k)}{\varepsilon_k}\sin(\varepsilon_kt) & \cos(\varepsilon_kt)-i\frac{h_z(k)-\omega/2}{\varepsilon_k}\sin(\varepsilon_kt)\end{pmatrix}.
\end{aligned} \tag{C2}$$

Using the above equation, we arrive at

$$U_F(t) = e^{-it[h_z(k)-h]}\begin{pmatrix} \left[\cos(\varepsilon_k t) + i\frac{h_z(k)-\omega/2}{\varepsilon_k}\sin(\varepsilon_k t)\right]e^{i\omega t/2} & \frac{h_{xy}(k)}{\varepsilon_k}\sin(\varepsilon_k t)e^{i\omega t/2} & 0 & 0 \\ -\frac{h_{xy}(k)}{\varepsilon_k}\sin(\varepsilon_k t)e^{i\omega t/2} & \left[\cos(\varepsilon_k t) - i\frac{h_z(k)-\omega/2}{\varepsilon_k}\sin(\varepsilon_k t)\right]e^{i\omega t/2} & 0 & 0 \\ 0 & 0 & 1 & 0 \\ 0 & 0 & 0 & 1 \end{pmatrix}, \tag{C3}$$

and the time evolution operator is given by

$$U_k(t) = e^{-it[h_z(k)-h]}\begin{pmatrix} \left[\cos(\varepsilon_k t) + i\frac{h_z(k)-\omega/2}{\varepsilon_k}\sin(\varepsilon_k t)\right]e^{i\omega t/2} & \frac{h_{xy}(k)}{\varepsilon_k}\sin(\varepsilon_k t)e^{i\omega t/2} & 0 & 0 \\ -\frac{h_{xy}(k)}{\varepsilon_k}\sin(\varepsilon_k t)e^{-i\omega t/2} & \left[\cos(\varepsilon_k t) - i\frac{h_z(k)-\omega/2}{\varepsilon_k}\sin(\varepsilon_k t)\right]e^{-i\omega t/2} & 0 & 0 \\ 0 & 0 & 1 & 0 \\ 0 & 0 & 0 & 1 \end{pmatrix}. \tag{C4}$$

Similarly, the initial mixed state density matrix of the Floquet system in thermal equilibrium with a heat bath, corresponding to $\mathcal{H}_k$ is

$$\rho_k(0) = \frac{e^{-\beta\mathcal{H}_k}}{\mathrm{Tr}(e^{-\beta\mathcal{H}_k})} = \frac{1}{2[\cosh(\beta\varepsilon_k)e^{\beta\omega/2}+1]} \times \begin{pmatrix} \left[\cosh(\beta\varepsilon_k) + \frac{h_z(k)-\omega/2}{\varepsilon_k}\sinh(\beta\varepsilon_k)\right]e^{\beta\omega/2} & -i\frac{h_{xy}(k)}{\varepsilon_k}\sinh(\beta\varepsilon_k)e^{\beta\omega/2} & 0 & 0 \\ i\frac{h_{xy}(k)}{\varepsilon_k}\sinh(\beta\varepsilon_k)e^{\beta\omega/2} & \left[\cosh(\beta\varepsilon_k) - \frac{h_z-\omega/2}{\varepsilon_k}\sinh(\beta\varepsilon_k)\right]e^{\beta\omega/2} & 0 & 0 \\ 0 & 0 & 1 & 0 \\ 0 & 0 & 0 & 1 \end{pmatrix}. \tag{C5}$$

Since the Hamiltonian is decomposable, one can find the density matrix at time t for the kth subspace, by solving the Liouville equation. Using Eqs. (C4) and (C5) and following the relation $\rho_k(t) = U_k(t)\rho_k(0)U_k^\dagger(t)$, one can conclude the density matrix at time t. To compute the OTOC we must first calculate $c_k^\dagger \pm c_{-k}$, $c_{-k}^\dagger \pm c_k$ as follows:

$$c_k^\dagger + c_{-k} = \begin{pmatrix} 0 & 0 & 0 & 1 \\ 0 & 0 & 0 & 1 \\ 1 & -1 & 0 & 0 \\ 0 & 0 & 0 & 0 \end{pmatrix}, \quad c_k^\dagger - c_{-k} = \begin{pmatrix} 0 & 0 & 0 & -1 \\ 0 & 0 & 0 & -1 \\ 1 & 1 & 0 & 0 \\ 0 & 0 & 0 & 0 \end{pmatrix},$$
$$c_{-k}^\dagger + c_k = \begin{pmatrix} 0 & 0 & 1 & 0 \\ 0 & 0 & -1 & 0 \\ 0 & 0 & 0 & 0 \\ 1 & 1 & 0 & 0 \end{pmatrix}, \quad c_{-k}^\dagger - c_k = \begin{pmatrix} 0 & 0 & -1 & 0 \\ 0 & 0 & -1 & 0 \\ 0 & 0 & 0 & 0 \\ 1 & -1 & 0 & 0 \end{pmatrix}. \tag{C6}$$

Then, by considering Eq. (4), and the above equations, time-dependent correlation functions are obtained. Finally, following the procedure of the Pffafian method (Secs. II B and II C), one would compute the local and nonlocal OTOCs (Fig. 11).

APPENDIX D: EXACT SOLUTION OF THE SYNCHRONIZED FLOQUET XY MODEL

Applying Jordan-Wigner as well as Fourier transformations on Eq. (12), and within the antiperiodic boundary condition used to minimize boundary effects, the Hamiltonian in terms of fermionic creation and annihilation operators is identical to

$$H(t) = \sum_{k>0}\{2[-J(t)\cos(k) - h(t)](c_k^\dagger c_k - c_{-k}c_{-k}^\dagger) - 2[iJ(t)\gamma\sin(k)](c_k^\dagger c_{-k}^\dagger + c_k c_{-k})\}. \tag{D1}$$

The resulting Hamiltonian can be written as $H(t) = \sum_{k>0} H_k(t)$, where the local Hamiltonian reads

$$H_k(t) = h_z(k,t)(c_k^\dagger c_k + c_{-k}^\dagger c_{-k}) - ih_{xy}(k,t)(c_k^\dagger c_{-k}^\dagger + c_k c_{-k}), \tag{D2}$$

where $h_z(k,t) = -2J(t)\cos(k) - 2h(t)$, $h_{xy}(k,t) = 2J(t)\gamma\sin(k)$ and the wave number k is equal to $k = (2p-1)\pi/N$ and the integer p runs from $-N/2+1$ to $N/2$, where N is the total number of spins (sites) in the chain. Hence, $H_k(t)$ can be diagonalized using the procedure of Bogoliubov transformation, which is given by

$$\begin{aligned} c_k &= u_k\gamma_k + iv_k\gamma_{-k}^\dagger, \\ c_{-k} &= u_k\gamma_{-k} - iv_k\gamma_k^\dagger, \\ c_k^\dagger &= u_k\gamma_k^\dagger - iv_k\gamma_{-k}, \\ c_{-k}^\dagger &= u_k\gamma_{-k}^\dagger + iv_k\gamma_k. \end{aligned} \tag{D3}$$

The Bogoliubov transformation completes the diagonalization of Hamiltonian as

$$H_k(t) = \sum_{k>0}\Delta_k(t)\left(\gamma_k^\dagger\gamma_k - \frac{1}{2}\right), \tag{D4}$$

where $\Delta_k(t) = \{[h_z(k,t)]^2 + [h_{xy}(k,t)]^2\}^{1/2}$ is the dispersion of elementary excitations and by considering $u_k(t) = \cos[\theta_k(t)/2]$ and $v_k(t) = \sin[\theta_k(t)/2]$, the Bogoliubov angle

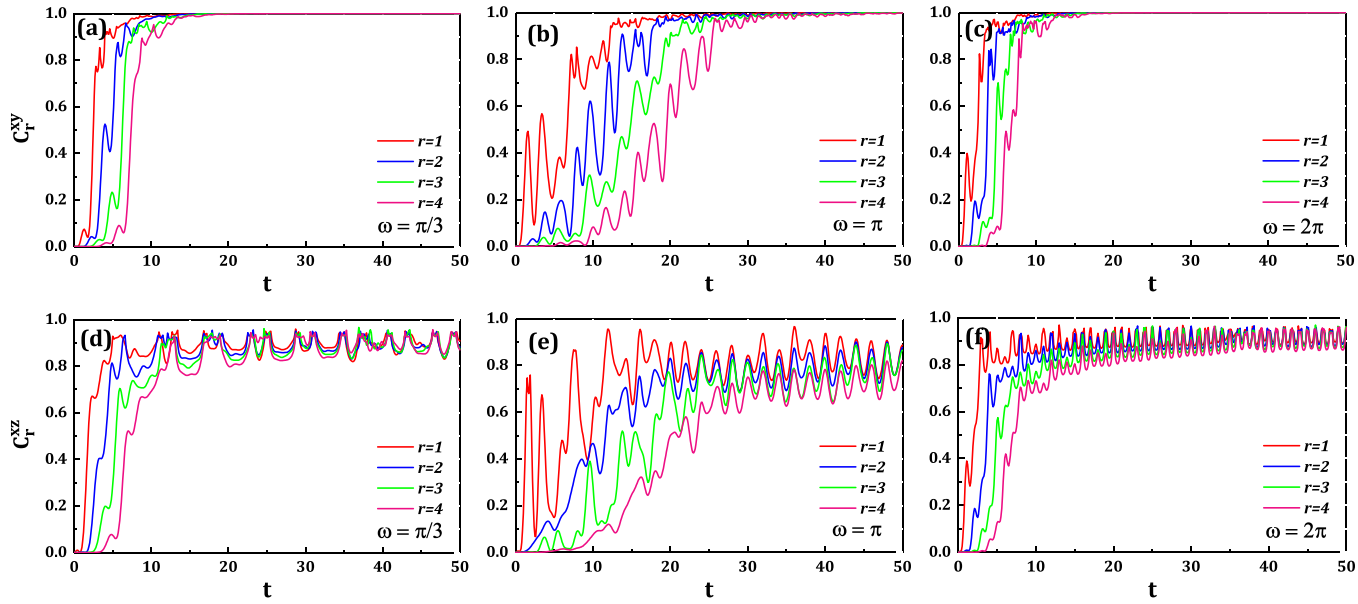

FIG. 11. Time evolution of C_r^{xy} and C_r^{xz} for several fixed separations in the Floquet XY model, with $\beta = 0$ and different values of ω. We consider $N = 100$, and the Hamiltonian parameters are $J = 0.25\pi$, $h = 0.5\pi$, and $\gamma = 0.5$.

$\theta_k(t)$ satisfies the relation $\tan[\theta_k(t)] = -\frac{h_{xy}(k,t)}{h_z(k,t)}$. The ground state (Bogoliubov vacuum), the state that is annihilated by γ_k, and the excited state of the above Hamiltonian, for antiperiodic boundary conditions, are given by

$$|\Psi_0^{ap}\rangle = \Pi_k\{\cos[\theta_k(t)/2] + i\sin[\theta_k(t)/2]c_k^\dagger c_{-k}^\dagger\}|0\rangle,$$
$$|\Psi_1^{ap}\rangle = \Pi_k\{i\sin[\theta_k(t)/2] + \cos[\theta_k(t)/2]c_k^\dagger c_{-k}^\dagger\}|0\rangle, \quad \text{(D5)}$$

where $|0\rangle$ is the vacuum of the system. For the synchronized model [$J(t) = \lambda h(t)$], that we consider afterward, we have $h_z(k,t) = -h(t)P(k)$, $h_{xy}(k,t) = h(t)Q(k)$, $\Delta_k(t) = h(t)\epsilon_k$, and $\tan[\theta_k'(t)] = \frac{Q(k)}{P(k)}$, in which $P(k) = 2\lambda\cos(k) - 2$, $Q(k) = 2\lambda\gamma\sin(k)$, and $\epsilon_k = \{[P(k)]^2 + [Q(k)]^2\}^{1/2}$ are time independent. Moreover, we focus on the case of the harmonically time-dependent magnetic field $h(t) = h_0 + h_1\cos(\omega t)$.

In the Bogoliubov basis [Eq. (D5)], the Hamiltonian $H_k(t)$, density matrix $\rho_k(0)$, and time evolution operator $U_k(t)$ are expressed as

$$H_k(t) = h(t)\begin{pmatrix} -\frac{\epsilon_k}{2} & 0 \\ 0 & \frac{\epsilon_k}{2} \end{pmatrix}, \quad \text{(D6)}$$

$$U_k(t) = \begin{pmatrix} e^{i(\epsilon_k/2)\tau} & 0 \\ 0 & e^{-i(\epsilon_k/2)\tau} \end{pmatrix}, \quad \text{(D7)}$$

$$\rho_k(0) = \frac{1}{2\cosh\left[\beta h(0)\frac{\epsilon_k}{2}\right]}\begin{pmatrix} e^{\beta h(0)(\epsilon_k/2)} & 0 \\ 0 & e^{-\beta h(0)(\epsilon_k/2)} \end{pmatrix}, \quad \text{(D8)}$$

where $\tau = \int_0^t h(t')dt'$, and the density matrix at time t is obtained to be $\rho_k(t) = U_k(t)\rho_k(0)U_k(t)$.

APPENDIX E: OTOC IN SYNCHRONIZED XY CHAIN

Considering Eq. (D3), we obtain

$$c_k^\dagger + c_{-k} = e^{-i\theta_k'/2}(\gamma_k^\dagger + \gamma_{-k}),$$
$$c_k^\dagger - c_{-k} = e^{i\theta_k'/2}(\gamma_k^\dagger - \gamma_{-k}),$$
$$c_{-k}^\dagger + c_k = e^{i\theta_k'/2}(\gamma_{-k}^\dagger + \gamma_k),$$
$$c_{-k}^\dagger - c_k = e^{-i\theta_k'/2}(\gamma_{-k}^\dagger - \gamma_k). \quad \text{(E1)}$$

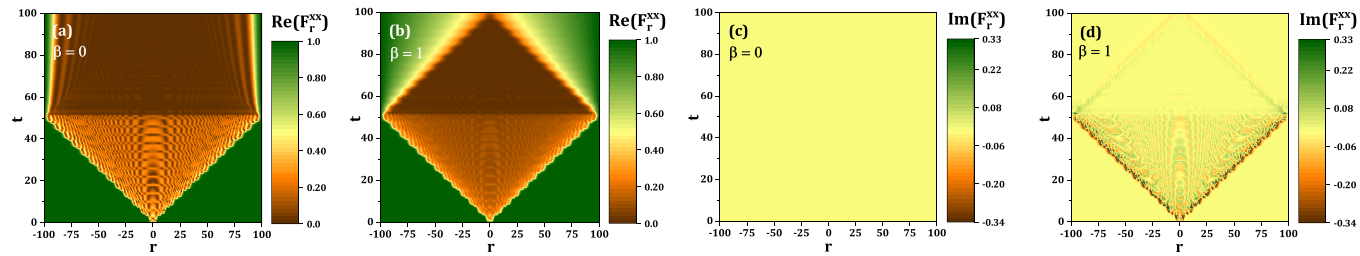

FIG. 12. Density plot of the real and imaginary parts of F_r^{xx} versus time and separation, for the synchronized Ising model, in the presence of $h(t) = h_0 + h_1\cos(\omega t)$ for inverse temperature $\beta = 0$ and $\beta = 1$. We consider $N = 200$ and strong coupling $\lambda = 1$, and the other parameters are $h_0 = 1$, $h_1 = 1$, and $\omega = \pi/2$.

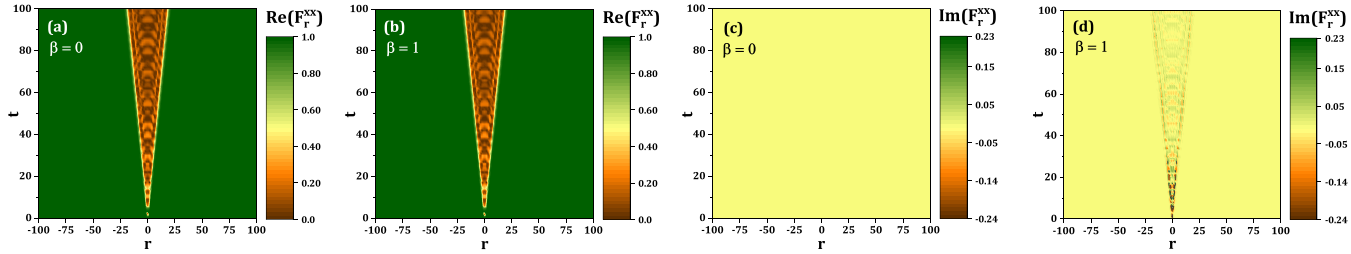

FIG. 13. Density plot of the real and imaginary parts of F_r^{xx} versus time and separation, for the synchronized Ising model, in the presence of $h(t) = h_0 + h_1 \cos(\omega t)$ for inverse temperature $\beta = 0$ and $\beta = 1$. We consider $N = 200$ and weak coupling $\lambda = 0.1$, and the other parameters are $h_0 = 1,\ h_1 = 1,$ and $\omega = \pi/2$.

Then using Eq. (4) we get

$$\langle A_p(t)A_q\rangle = \frac{1}{N}\sum_k e^{ik(p-q)} \times \langle U_{1k}^\dagger(t)(\gamma_k^\dagger + \gamma_{-k})U_{1k}(t)(\gamma_{-k}^\dagger + \gamma_k)\rangle,$$

$$\langle A_p(t)B_q\rangle = \frac{1}{N}\sum_k e^{ik(p-q)}e^{-i\theta_k'} \times \langle U_{1k}^\dagger(t)(\gamma_k^\dagger + \gamma_{-k})U_{1k}(t)(\gamma_{-k}^\dagger - \gamma_k)\rangle,$$

$$\langle B_p(t)A_q\rangle = \frac{1}{N}\sum_k e^{ik(p-q)}e^{i\theta_k'} \times \langle U_{1k}^\dagger(t)(\gamma_k^\dagger - \gamma_{-k})U_{1k}(t)(\gamma_{-k}^\dagger + \gamma_k)\rangle,$$

$$\langle B_p(t)B_q\rangle = \frac{1}{N}\sum_k e^{ik(p-q)} \times \langle U_{1k}^\dagger(t)(\gamma_k^\dagger - \gamma_{-k})U_{1k}(t)(\gamma_{-k}^\dagger - \gamma_k)\rangle. \tag{E2}$$

Finally, following the above equations and considering Eqs. (D6)–(D8), time-dependent correlation functions for the mixed state synchronized case are given by

$$\langle A_p(t)A_q\rangle = \frac{1}{N}\sum_k e^{ik(p-q)} \times \left\{\cos(\epsilon_k\tau) - i\sin(\epsilon_k\tau)\tanh\left[\beta h(0)\frac{\epsilon_k}{2}\right]\right\},$$

$$\langle A_p(t)B_q\rangle = \frac{1}{N}\sum_k e^{ik(p-q)}e^{-i\theta_k'} \times \left\{\cos(\epsilon_k\tau)\tanh\left[\beta h(0)\frac{\epsilon_k}{2}\right] - i\sin(\epsilon_k\tau)\right\},$$

$$\langle B_p(t)A_q\rangle = -\frac{1}{N}\sum_k e^{ik(p-q)}e^{i\theta_k'} \times \left\{\cos(\epsilon_k\tau)\tanh\left[\beta h(0)\frac{\epsilon_k}{2}\right] - i\sin(\epsilon_k\tau)\right\},$$

$$\langle B_p(t)B_q\rangle = -\frac{1}{N}\sum_k e^{ik(p-q)} \times \left\{\cos(\epsilon_k\tau) - i\sin(\epsilon_k\tau)\tanh\left[\beta h(0)\frac{\epsilon_k}{2}\right]\right\}. \tag{E3}$$

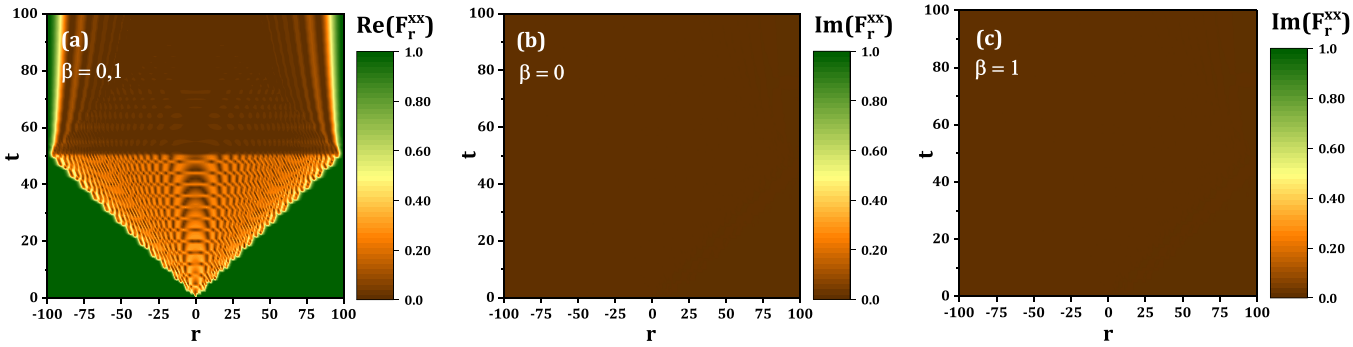

FIG. 14. Density plot of the real and imaginary parts of F_r^{xx} versus time and separation, for the synchronized Ising model, in the presence of $h(t) = h_0 + h_1\cos(\omega t)$ where $h_0 = 1, h_1 = -1, \omega = \pi/2$, i.e., $h(t = 0) = 0$. (a) The real part of F_r^{xx} is the same for $\beta = 0$ and $\beta = 1$. The imaginary part of F_r^{xx} is plotted for inverse temperature (b) $\beta = 0$ and (c) $\beta = 1$. The system is in the strong coupling $\lambda = 1$ and $N = 200$.

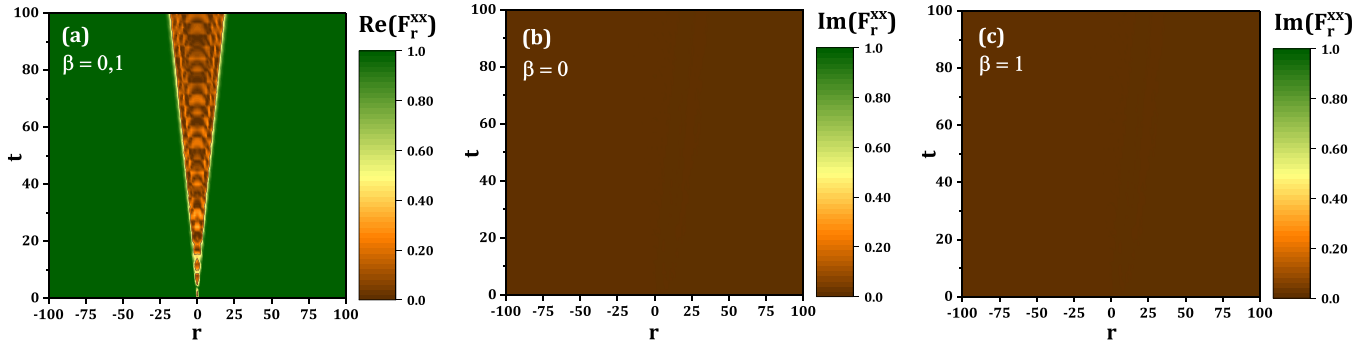

FIG. 15. The explanation is the same as for Fig. 14, except the coupling $\lambda = 0.1$, which is weak.

OTOC of nonlocal operators in the synchronized Floquet XY model

The general behavior of the OTOC comprised of nonlocal operators for the synchronized Ising model, is illustrated in Figs. 12–15, using the procedure described in Sec. II, for $N = 200$. As seen, the xx OTOC shows the signature of operator spreading, although with some differences in comparison with the zz OTOC. Figures 12 and 13 exhibit the evolution of the real and imaginary parts of F_r^{xx} in time, at high and low temperature and for the $h(0) \neq 0$ case.

The OTOC with nonlocal operators has been depicted in Figs. 14 and 15 for the $h(0) = 0$ case. As can be observed, the diagrams reveal no temperature dependence and so decreasing the temperature from its infinite value, does not significantly alter the quantitative behavior of the OTOC in this context. Hence, similar to the situation of C_r^{zz}, when the initial time magnetic field is zero, vanishing of the imaginary part of F_r^{xx} signals the occurrence of a FDQPT independent of temperature, which is in agreement with the results of the Loschmidt amplitude analysis. So, it would be suitable to detect the mixed state FDQPT of the synchronized Ising chain due to analyzing the vanishing of $\mathrm{Im}(F_r^{zz})$ as well as $\mathrm{Im}(F_r^{xx})$ at any temperature.

[1] X. Nie, B.-B. Wei, X. Chen, Z. Zhang, X. Zhao, C. Qiu, Y. Tian, Y. Ji, T. Xin, D. Lu, and J. Li, Phys. Rev. Lett. **124**, 250601 (2020).

[2] B. Swingle, G. Bentsen, M. Schleier-Smith, and P. Hayden, Phys. Rev. A **94**, 040302(R) (2016).

[3] G. Zhu, M. Hafezi, and T. Grover, Phys. Rev. A **94**, 062329 (2016).

[4] A. M. Kaufman, M. E. Tai, A. Lukin, M. Rispoli, R. Schittko, P. M. Preiss, and M. Greiner, Science **353**, 794 (2016).

[5] M. Gärttner, J. G. Bohnet, A. Safavi-Naini, M. L. Wall, J. J. Bollinger, and A. M. Rey, Nat. Phys. **13**, 781 (2017).

[6] J. Li, R. Fan, H. Wang, B. Ye, B. Zeng, H. Zhai, X. Peng, and J. Du, Phys. Rev. X **7**, 031011 (2017).

[7] R. J. Lewis-Swan, A. Safavi-Naini, J. J. Bollinger, and A. M. Rey, Nat. Commun. **10**, 1581 (2019).

[8] K. X. Wei, C. Ramanathan, and P. Cappellaro, Phys. Rev. Lett. **120**, 070501 (2018).

[9] D. A. Roberts and B. Swingle, Phys. Rev. Lett. **117**, 091602 (2016).

[10] D. J. Luitz and Y. Bar Lev, Phys. Rev. B **96**, 020406(R) (2017).

[11] E. Iyoda and T. Sagawa, Phys. Rev. A **97**, 042330 (2018).

[12] C. W. von Keyserlingk, T. Rakovszky, F. Pollmann, and S. L. Sondhi, Phys. Rev. X **8**, 021013 (2018).

[13] M. Niknam, L. F. Santos, and D. G. Cory, Phys. Rev. Res. **2**, 013200 (2020).

[14] Y. Alavirad and A. Lavasani, Phys. Rev. A **99**, 043602 (2019).

[15] P. Hosur, X.-L. Qi, D. A. Roberts, and B. Yoshida, J. High Energy Phys. 02 (2016) 004.

[16] B. Swingle and D. Chowdhury, Phys. Rev. B **95**, 060201(R) (2017).

[17] M. Schleier-Smith, Nat. Phys. **13**, 724 (2017).

[18] S. Pappalardi, A. Russomanno, B. Žunkovič, F. Iemini, A. Silva, and R. Fazio, Phys. Rev. B **98**, 134303 (2018).

[19] M. J. Klug, M. S. Scheurer, and J. Schmalian, Phys. Rev. B **98**, 045102 (2018).

[20] V. Khemani, A. Vishwanath, and D. A. Huse, Phys. Rev. X **8**, 031057 (2018).

[21] J. Maldacena, S. H. Shenker, and D. Stanford, J. High Energy Phys. 08 (2016) 106.

[22] S. H. Shenker and D. Stanford, J. High Energy Phys. 03 (2014) 067.

[23] A. Kitaev and S. J. Suh, J. High Energy Phys 05 (2018) 183.

[24] R. Fan, P. Zhang, H. Shen, and H. Zhai, Sci. Bull. **62**, 707 (2017).

[25] A. Larkin and Y. N. Ovchinnikov, Sov. Phys. JETP **28**, 1200 (1969).

[26] K. K. Sharma and V. P. Gerdt, Quantum Inf. Proc. **20**, 195 (2021).

[27] S. I. Doronin, E. B. Fel'dman, and I. D. Lazarev, Phys. Rev. A **100**, 022330 (2019).

[28] I. Kukuljan, S. Grozdanov, and T. Prosen, Phys. Rev. B **96**, 060301(R) (2017).

[29] K. Hashimoto, K. Murata, and R. Yoshii, J. High Energy Phys. 10 (2017) 138.

[30] E. B. Rozenbaum, S. Ganeshan, and V. Galitski, Phys. Rev. Lett. **118**, 086801 (2017).

[31] E. B. Rozenbaum, S. Ganeshan, and V. Galitski, Phys. Rev. B **100**, 035112 (2019).

[32] I. García-Mata, M. Saraceno, R. A. Jalabert, A. J. Roncaglia, and D. A. Wisniacki, Phys. Rev. Lett. **121**, 210601 (2018).

[33] E. J. Torres-Herrera, A. M. García-García, and L. F. Santos, Phys. Rev. B **97**, 060303(R) (2018).

[34] J. Chávez-Carlos, B. López-del-Carpio, M. A. Bastarrachea-Magnani, P. Stránský, S. Lerma-Hernández, L. F. Santos, and J. G. Hirsch, Phys. Rev. Lett. **122**, 024101 (2019).

[35] J. Maldacena, D. Stanford, and Z. Yang, Fortschr. Phys. **65**, 1700034 (2017).

[36] J. Maldacena and D. Stanford, Phys. Rev. D **94**, 106002 (2016).

[37] A. A. Patel, D. Chowdhury, S. Sachdev, and B. Swingle, Phys. Rev. X **7**, 031047 (2017).

[38] B. Dóra and R. Moessner, Phys. Rev. Lett. **119**, 026802 (2017).

[39] H. Shen, P. Zhang, R. Fan, and H. Zhai, Phys. Rev. B **96**, 054503 (2017).

[40] M. Heyl, F. Pollmann, and B. Dóra, Phys. Rev. Lett. **121**, 016801 (2018).

[41] S. Sahu, S. Xu, and B. Swingle, Phys. Rev. Lett. **123**, 165902 (2019).

[42] M. Campisi and J. Goold, Phys. Rev. E **95**, 062127 (2017).

[43] A. Chenu, I. L. Egusquiza, J. Molina-Vilaplana, and A. del Campo, Sci. Rep. **8**, 12634 (2018).

[44] A. A. Patel and S. Sachdev, Proc. Natl. Acad. Sci. USA **114**, 1844 (2017).

[45] C.-J. Lin and O. I. Motrunich, Phys. Rev. B **98**, 134305 (2018).

[46] J. Riddell and E. S. Sørensen, Phys. Rev. B **99**, 054205 (2019).

[47] M. McGinley, A. Nunnenkamp, and J. Knolle, Phys. Rev. Lett. **122**, 020603 (2019).

[48] D. Chowdhury and B. Swingle, Phys. Rev. D **96**, 065005 (2017).

[49] B. Yan, L. Cincio, and W. H. Zurek, Phys. Rev. Lett. **124**, 160603 (2020).

[50] W. Buijsman, V. Gritsev, and R. Sprik, Phys. Rev. Lett. **118**, 080601 (2017).

[51] S. Ray, S. Sinha, and K. Sengupta, Phys. Rev. A **98**, 053631 (2018).

[52] Y. Huang, Y.-L. Zhang, and X. Chen, Ann. Phys. **529**, 1600318 (2017).

[53] Q. Wang and F. Pérez-Bernal, Phys. Rev. A **100**, 062113 (2019).

[54] C. M. Lóbez and A. Relaño, Phys. Rev. E **94**, 012140 (2016).

[55] C. B. Dağ, K. Sun, and L.-M. Duan, Phys. Rev. Lett. **123**, 140602 (2019).

[56] B.-B. Wei, G. Sun, and M.-J. Hwang, Phys. Rev. B **100**, 195107 (2019).

[57] J.-H. Bao and C.-Y. Zhang, Commun. Theor. Phys. **72**, 085103 (2020).

[58] C.-J. Lin and O. I. Motrunich, Phys. Rev. B **97**, 144304 (2018).

[59] B. Swingle, Nat. Phys. **14**, 988 (2018).

[60] N. Lashkari, D. Stanford, M. Hastings, T. Osborne, and P. Hayden, J. High Energy Phys. 04 (2013) 022.

[61] Y. Sekino and L. Susskind, J. High Energy Phys. 10 (2008) 065.

[62] K. Slagle, Z. Bi, Y.-Z. You, and C. Xu, Phys. Rev. B **95**, 165136 (2017).

[63] E. Lieb, T. Schultz, and D. Mattis, Ann. Phys. **16**, 407 (1961).

[64] E. Barouch, B. M. McCoy, and M. Dresden, Phys. Rev. A **2**, 1075 (1970).

[65] E. Barouch and B. M. McCoy, Phys. Rev. A **3**, 786 (1971).

[66] E. Eriksson and H. Johannesson, Phys. Rev. B **79**, 224424 (2009).

[67] I. Titvinidze and G. Japaridze, Eur. Phys. J. B **32**, 383 (2003).

[68] R. Jafari, Phys. Rev. B **84**, 035112 (2011).

[69] R. Jafari, Eur. Phys. J. B **85**, 167 (2012).

[70] S. Mahdavifar, S. Mahdavifar, and R. Jafari, Phys. Rev. A **96**, 052303 (2017).

[71] A. Chapman and A. Miyake, Phys. Rev. A **98**, 012309 (2018).

[72] D. Rossini, S. Suzuki, G. Mussardo, G. E. Santoro, and A. Silva, Phys. Rev. B **82**, 144302 (2010).

[73] S. Sachdev, *Handbook of Magnetism and Advanced Magnetic Materials* (Wiley-Interscience, New York, 2007).

[74] B. M. McCoy, E. Barouch, and D. B. Abraham, Phys. Rev. A **4**, 2331 (1971).

[75] A. Cayley, *Note on the Theory of Permutations* (Taylor & Francis, 1849), Vol. 34, pp. 527–529.

[76] F. H. L. Essler and M. Fagotti, J. Stat. Mech.: Theory Exp. (2016) 064002.

[77] S. Aditya, S. Samanta, A. Sen, K. Sengupta, and D. Sen, arXiv:2112.02915.

[78] M. Heyl, A. Polkovnikov, and S. Kehrein, Phys. Rev. Lett. **110**, 135704 (2013).

[79] M. Heyl, Rep. Prog. Phys. **81**, 054001 (2018).

[80] M. Sadrzadeh, R. Jafari, and A. Langari, Phys. Rev. B **103**, 144305 (2021).

[81] P. Uhrich, N. Defenu, R. Jafari, and J. C. Halimeh, Phys. Rev. B **101**, 245148 (2020).

[82] J. C. Halimeh and V. Zauner-Stauber, Phys. Rev. B **96**, 134427 (2017).

[83] A. Zvyagin, Low Temp. Phys. **42**, 971 (2016).

[84] K. Yang, L. Zhou, W. Ma, X. Kong, P. Wang, X. Qin, X. Rong, Y. Wang, F. Shi, J. Gong, and J. Du, Phys. Rev. B **100**, 085308 (2019).

[85] S. Zamani, R. Jafari, and A. Langari, Phys. Rev. B **102**, 144306 (2020).

[86] R. Jafari and A. Akbari, Phys. Rev. A **103**, 012204 (2021).

[87] J. K. Asbóth, Phys. Rev. B **86**, 195414 (2012).

[88] J. K. Asbóth and H. Obuse, Phys. Rev. B **88**, 121406(R) (2013).

[89] J. Naji, M. Jafari, R. Jafari, and A. Akbari, Phys. Rev. A **105**, 022220 (2022).

[90] R. Jafari, A. Akbari, U. Mishra, and H. Johannesson, arXiv:2111.09926.

[91] A. Sen, S. Nandy, and K. Sengupta, Phys. Rev. B **94**, 214301 (2016).

[92] R. Jafari, H. Johannesson, A. Langari, and M. A. Martin-Delgado, Phys. Rev. B **99**, 054302 (2019).

[93] R. Jafari, Sci. Rep. **9**, 2871 (2019).

[94] R. Jafari and H. Johannesson, Phys. Rev. Lett. **118**, 015701 (2017).

[95] U. Divakaran, Phys. Rev. E **88**, 052122 (2013).

[96] K. Najafi, M. A. Rajabpour, and J. Viti, J. Stat. Mech.: Theory Exp. (2019) 083102.

[97] T. V. Zache, N. Mueller, J. T. Schneider, F. Jendrzejewski, J. Berges, and P. Hauke, Phys. Rev. Lett. **122**, 050403 (2019).

[98] M. Serbyn and D. A. Abanin, Phys. Rev. B **96**, 014202 (2017).

[99] W. C. Yu, P. D. Sacramento, Y. C. Li, and H.-Q. Lin, Phys. Rev. B **104**, 085104 (2021).

[100] N. Fläschner, D. Vogel, M. Tarnowski, B. Rem, D.-S. Lühmann, M. Heyl, J. Budich, L. Mathey, K. Sengstock, and C. Weitenberg, Nat. Phys. **14**, 265 (2018).

[101] P. Jurcevic, H. Shen, P. Hauke, C. Maier, T. Brydges, C. Hempel, B. P. Lanyon, M. Heyl, R. Blatt, and C. F. Roos, Phys. Rev. Lett. **119**, 080501 (2017).

[102] U. Bhattacharya, S. Bandyopadhyay, and A. Dutta, Phys. Rev. B **96**, 180303(R) (2017).

[103] M. Heyl and J. C. Budich, Phys. Rev. B **96**, 180304(R) (2017).

[104] T. Nag, D. Sen, and A. Dutta, Phys. Rev. A **91**, 063607 (2015).